A theory of germinal center B cell selection, division, and exit

Meyer-Hermann, Michael; Mohr, Elodie; Pelletier, Nadége; Zhang, Yang; Victora, Gabriel D; Toellner, Kai-Michael

DOI:
10.1016/j.celrep.2012.05.010

Please cite this article in press as: Meyer-Hermann et al., A Theory of Germinal Center B Cell Selection, Division, and Exit, Cell Reports (2012), http://dx.doi.org/10.1016/j.celrep.2012.05.010

Cell Reports
Article

A Theory of Germinal Center B Cell Selection, Division, and Exit

Michael Meyer-Hermann,[1,2,*] Elodie Mohr,[3] Nadége Pelletier,[4] Yang Zhang,[5] Gabriel D. Victora,[6,7] and Kai-Michael Toellner[5,7]

[1]Department for Systems Immunology, Helmholtz Centre for Infection Research, Inhoffenstrasse 7, 38124 Braunschweig, Germany
[2]Bio Center for Life Sciences, Technische Universität Braunschweig, Spielmannstrasse 7, 38106 Braunschweig, Germany
[3]Instituto Gulbenkian de Ciência, Rua da Quinta Grande 6, Apartado 14, PT-2781-901 Oeiras, Portugal
[4]Department of Immunology and Microbial Sciences, The Scripps Research Institute, La Jolla, CA 92037, USA
[5]School of Immunity and Infection, University of Birmingham Medical School, Birmingham B15 2TT, UK
[6]Whitehead Institute for Biomedical Research, Nine Cambridge Center, Cambridge, MA 02142, USA
[7]These authors contributed equally to this work
*Correspondence: michael.meyer-hermann@helmholtz-hzi.de
http://dx.doi.org/10.1016/j.celrep.2012.05.010

SUMMARY

High-affinity antibodies are generated in germinal centers in a process involving mutation and selection of B cells. Information processing in germinal center reactions has been investigated in a number of recent experiments. These have revealed cell migration patterns, asymmetric cell divisions, and cell-cell interaction characteristics, used here to develop a theory of germinal center B cell selection, division, and exit (the LEDA model). According to this model, B cells selected by T follicular helper cells on the basis of successful antigen processing always return to the dark zone for asymmetric division, and acquired antigen is inherited by one daughter cell only. Antigen-retaining B cells differentiate to plasma cells and leave the germinal center through the dark zone. This theory has implications for the functioning of germinal centers because compared to previous models, high-affinity antibodies appear one day earlier and the amount of derived plasma cells is considerably larger.

INTRODUCTION

Germinal centers (GCs) are microanatomical structures that emerge in B cell (BC) follicles of secondary lymphoid tissue in response to T cell (TC)-dependent antigenic challenges (MacLennan, 1994). Within these structures, BCs undergo somatic hypermutation of their antibody variable regions (Berek and Milstein, 1987; Berek et al., 1991; Jacob et al., 1991; Dunn-Walters et al., 2002). These mutated BC receptors are then tested against antigen retained on the surface of GC resident follicular dendritic cells (FDCs) (Kosco-Vilbois, 2003). In a Darwinian process of random mutation and selection, BC-encoding antibodies with higher affinity to this antigen are identified and expanded. This process is termed *affinity maturation* of antibodies and is a remarkable property of adaptive immunity and BC biology.

The GC is divided into two functionally distinct zones, a dark zone (DZ), where BCs proliferate, and a light zone (LZ), characterized by the presence of FDCs and bound antigen and which is associated with BC selection (MacLennan, 1994; Camacho et al., 1998; Victora and Nussenzweig, 2012). During affinity maturation, BCs traffic between the two zones, alternating phases of division and mutation in the DZ with phases of affinity-dependent selection by antigen in the LZ, which leads to iterative optimization of antibodies. This model, known as cyclic re-entry, was predicted from control theory (Kepler and Perelson, 1993). Mathematical modeling further predicted that unequivocal detection of BC recycling would require tracking BCs in vivo for several hours (Figge et al., 2008; Meyer-Hermann et al., 2009). This prediction was confirmed in experiments in which BCs were labeled in either DZ or LZ by photoactivation (Victora et al., 2010). Data from these experiments are used in this study to quantitatively determine how dominant recycling in GCs really is.

Selection mechanisms contributing to affinity maturation in GCs have been a matter of controversy for many years. While it is likely that many mechanisms—such as competition for FDC binding sites (Keşmir and De Boer, 1999), a refractory time between two attempts to bind antigen (Meyer-Hermann et al., 2006), and masking of FDC-bound antigen by soluble antibodies (Tarlinton and Smith, 2000; Iber and Maini, 2002)—are orchestrated to induce affinity maturation, a dominant limiting role for T follicular helper cells (TFHs) was predicted by mathematical modeling (Meyer-Hermann et al., 2006; Meyer-Hermann, 2007) and confirmed by experiments (Victora et al., 2010; Schwickert et al., 2011). According to this selection model, high-affinity BC efficiently collect antigen from FDCs inferring higher density peptide MHC (pMHC) presentation that can be sensed by TFHs (Depoil et al., 2005; Fleire et al., 2006; Schwickert et al., 2011). These provide positive signals only to the BCs with highest pMHC. Positively selected BCs are presented with a choice of recycling for further mutation or exiting the GC reaction as memory or plasma cells (PCs) (Tarlinton and Smith, 2000). The extent to which this choice is influenced by TC help is unclear. Also unclear is the path of exit from GC taken by

Please cite this article in press as: Meyer-Hermann et al., A Theory of Germinal Center B Cell Selection, Division, and Exit, Cell Reports (2012), http://dx.doi.org/10.1016/j.celrep.2012.05.010

Cell PRESS
Open ACCESS

emerging PCs and whether PC-committed BCs further divide within the GC before exiting.

In view of the central relevance of GCs to adaptive immunity and vaccination, there has been tremendous effort to shed light on these specific aspects of the GC reaction, and mathematical modeling has become a natural and productive element of GC research. Here, we develop a consistent and comprehensive model of the GC reaction using a combined theoretical and experimental approach that integrates a large body of experimental data. In particular, the model predicts that cyclic re-entry is the dominant path of positively selected BCs, that TFHs control division and recycling frequency of GC BCs, that asymmetric division of GC BCs determines which BCs enter final differentiation, and that output cells leave the GC through the DZ. We present experimental data supporting the new GC selection, division, and exit model and propose new experiments capable of confirming it.

RESULTS

A mathematical model for the GC reaction was derived from a large body of key experimental data (for a detailed presentation, see Extended Experimental Procedures and Table S1). BC selection was based on a combination of competition for antigen-presenting FDC sites and affinity-dependent TC help. The BC motility model was derived from two-photon experiments (Allen et al., 2007; Figge et al., 2008). GC morphology, zoning (MacLennan, 1994; Camacho et al., 1998), population kinetics (Liu et al., 1991; Hollowood and Macartney, 1992), DZ-to-LZ ratio (Victora et al., 2010), and intravital imaging experiments that followed BCs in GCs for 1 (Allen et al., 2007; Schwickert et al., 2007; Hauser et al., 2007) or 6 hr (Victora et al., 2010) were used to validate the in silico model. Experiments providing antigen to GC BCs by targeting DEC205 were included, in particular, the fraction of DEC205$^{+/+}$ BCs and the rather specific oscillation of the DZ-to-LZ ratio, as well as the inhibition of affinity maturation and the increased PC output (Victora et al., 2010). Recent data showing asymmetric divisions of BCs (Thaunat et al., 2012; Barnett et al., 2012; Dustin and Meyer-Hermann, 2012) were also incorporated. These experiments were analyzed in four different models:

BASE assumes cyclic re-entry as the dominant pathway of positively selected BCs and that affinity-dependent help by TFH limits selection.

LEDA, in addition to BASE, assumes that BCs positively selected by TFHs retain the acquired antigen and always return to the DZ for division, where the retained antigen is distributed asymmetrically to both daughter cells (In association of asymmetric division, Leda in Greek mythology, gives birth to unequal, immortal and mortal, children). After division, all antigen-retaining BCs differentiate into PCs and LEave the GC through the DArk zone in direction of the T zone. BCs lacking antigen return to the LZ.

MIRE is the same model as BASE, but with MIddle REcycling level.

LORE is the same model as BASE, but with LOw REcycling level.

Defining the Reference Simulation

GC morphology exhibited a roundish DZ separated from a cap of LZ cells (Figure 1A) similar to data in (Camacho et al., 1998; Victora et al., 2010). BCs in a state of division and mutation (indicated by dark blue cells in Figure 1A), make up most of the DZ, whereas BCs in selection mode (indicated by green cells) are the main constituents of the LZ. Freshly selected BCs entering (but not necessarily completing) the cell cycle (indicated by light blue cells) are concentrated in the outer part of the LZ (Hardie et al., 1993).

GC volume kinetics were in qualitative agreement with in vivo data (Liu et al., 1991; Hollowood and Macartney, 1992) (Figure 1B). A quantitative comparison with these data would go beyond their accuracy because they were generated under different conditions. The GC population grew more slowly in the BASE model due to longer cell cycle and exhibited an unrealistic early drop in the LORE model.

BC Motility

In silico, BCs de- and resensitized for chemokines in a concentration-dependent manner (Extended Experimental Procedures). The resulting speed distribution (data not shown), the mean speed of $\approx$6 μm/min (compare to Figure 5E in Victora et al., 2010), and the reached distance curve including the size of the standard deviation were consistent with the data of Allen et al., 2007, for all models (Figure 1C for BASE). The reached distance is not sensitive to chemotaxis, which was active in all models (Meyer-Hermann et al., 2009; Beltman et al., 2011).

The DZ-to-LZ ratio was consistent with the value of 2.0 found in vivo (Figure 6C in Victora et al., 2010) in all in silico models (Figure 1D). The duration of the processes in both zones determined this ratio, which was increased by reduced selection pressure, leading to faster selection in the LZ, as well as prolonged division in the DZ. This counterintuitive in silico result is relevant for the correct interpretation of the photoactivation results discussed here.

Recycling

The recycling probability determines the proportion of positively selected BCs that re-enter cell cycle (90% in BASE) or differentiates to output (10% in BASE). The recycling probability has to be distinguished from the fraction of recycling events, defined as number of recycling events divided by all differentiation plus apoptosis events in LZ-BCs. This fraction was 25% (BASE and LEDA), 15% (MIRE), and 10% (LORE) (Figure 1E). Thus, BASE and LEDA stayed in the same range as the 30% estimated using a simplified model (Victora et al., 2010).

Affinity maturation was robust in all GC models and exhibited the takeover by high-affinity cells at Day 8 (Radmacher et al., 1998) (Figure 1F). Quantitatively, affinity was lower in LORE.

Photoactivation of GC BCs In Silico

In vivo photoactivation experiments revealed a clear asymmetry of transzone migration frequencies between the two GC zones (Figure 5D in Victora et al., 2010): While DZ-to-LZ migration was prominent, LZ-to-DZ migration was rare. Using an ordinary differential equation model, we found that this asymmetry is compatible with the cyclic re-entry model. However, the actual recycling probability of positively selected BCs could not be determined, and the saturation of DZ-to-LZ transzone migration

Cell PRESS
Open ACCESS

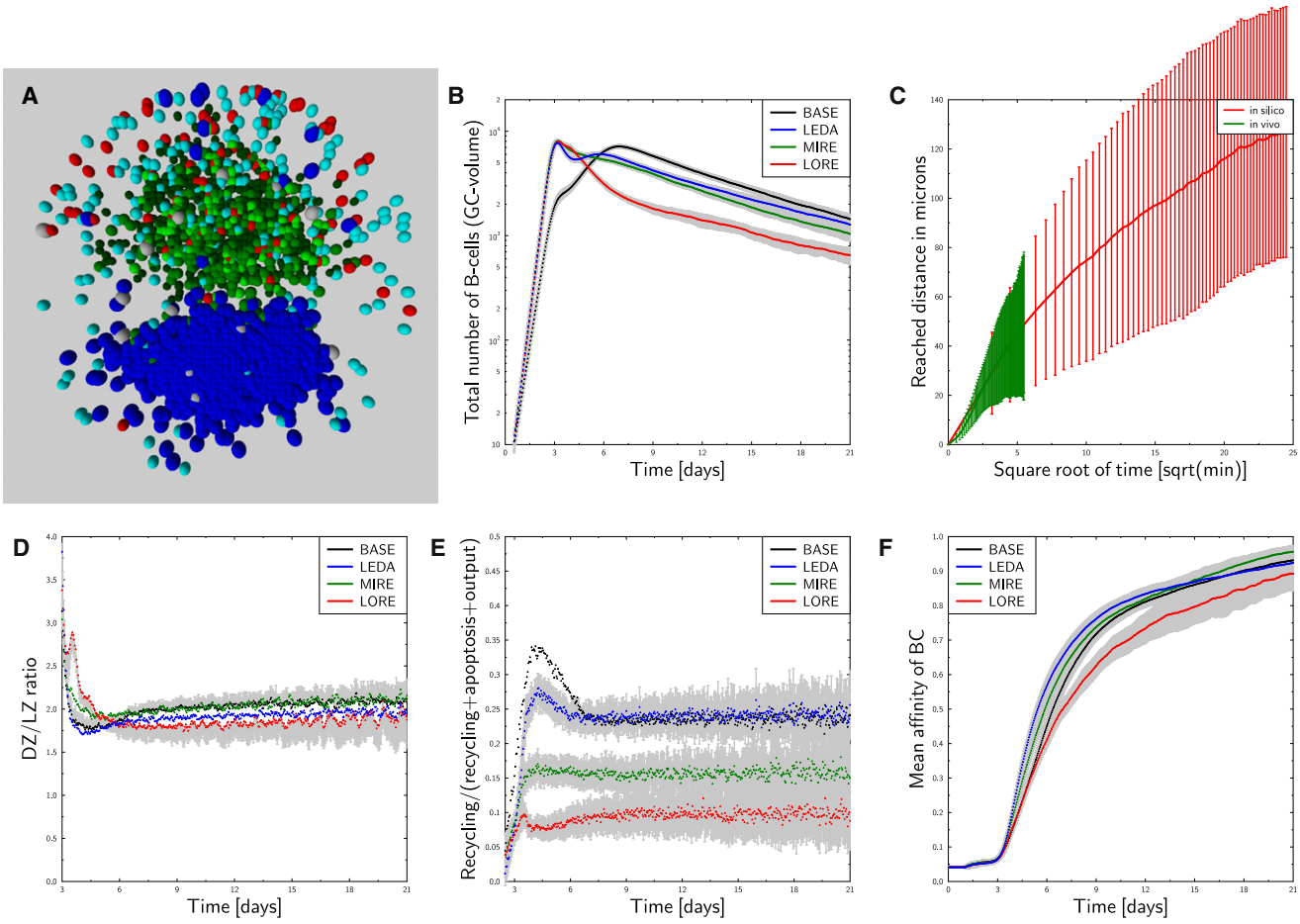

Figure 1. GC Characteristics In Silico

(A) Central slice of 50 μm of the BASE model GC at Day 5 after GC onset. The upper half of the GC is the LZ containing an FDC network (data not shown). Color code: Dividing CXCR4+ BC (dark blue), dividing CXCR4− BC (light blue), unselected nondividing BC (dark green), selected BC (light green), TFH (red), PC and memory cell (gray).

(B) Time course of GC volume for the BASE (black), LEDA (blue), MIRE (green), and LORE (red) models with 1 SD (N = 30, gray).

(C) Reached distance and SD for 1,000 dividing and 1,000 nondividing BCs tracked from Day 6 after GC onset for 10 hr in the BASE model (red) in comparison to the data from (Allen et al., 2007) (green).

(D) DZ-to-LZ ratio of GC BCs with a one-sided error bar for the BASE and LORE models. LEDA and MIRE errors were similar to BASE. Colors are as in (B).

(E) Fraction of recycling events among LZ BCs. Colors are as in (B).

(F) Mean affinity of GC BCs. Colors are as in (B).

at ~50% was not reproduced (Figure S4 in Victora et al., 2010). Having defined BASE as a reliable reference model, we were now in the position to address these questions with in silico photoactivation experiments (Figures 2A–2D).

Recycled BCs Start the Cell Cycle in the LZ

The asymmetry between the two directions of transzone migration found in vivo was confirmed in all four models (Figure 2C). A transient chemotaxis model (Figge et al., 2008) with concentration-dependent resensitization was assumed. Failure to allow cells to desensitize to the chemokines present in each zone resulted in cell clustering. Conversely, failure to allow cells to resensitize led to rapid reappearance in the opposite zone, thus suppressing a clear attribution of BC phenotypes to each GC zone and reducing the asymmetry of transzone migration.

A necessary requirement for the asymmetry of transzone migration in silico was that positively selected BCs enter cell cycle in the LZ. On one hand, the DZ-to-LZ ratio of 2 (Figure 1D) imposes that BCs must divide, on average, two times after each round of selection. On the other hand, DZ to LZ transzone migration frequency had to reach 50% in 4 hr. Even with the shortest cell cycle times of 6–8 hr compatible with experiments (Hanna, 1964; Zhang et al., 1988; Liu et al., 1991), insufficient BCs were available to leave the DZ within 4 hr if two full cell cycles were completed in the DZ. This contradiction was solved by allowing BCs to enter the cell cycle while still in the LZ, a condition that is supported by experimental data (Victora et al., 2010).

LZ BCs in cell cycle were located predominantly in the outer part of the LZ (Figure 1A, in cyan). BCs probing for antigen on

Please cite this article in press as: Meyer-Hermann et al., A Theory of Germinal Center B Cell Selection, Division, and Exit, Cell Reports (2012), http://dx.doi.org/10.1016/j.celrep.2012.05.010

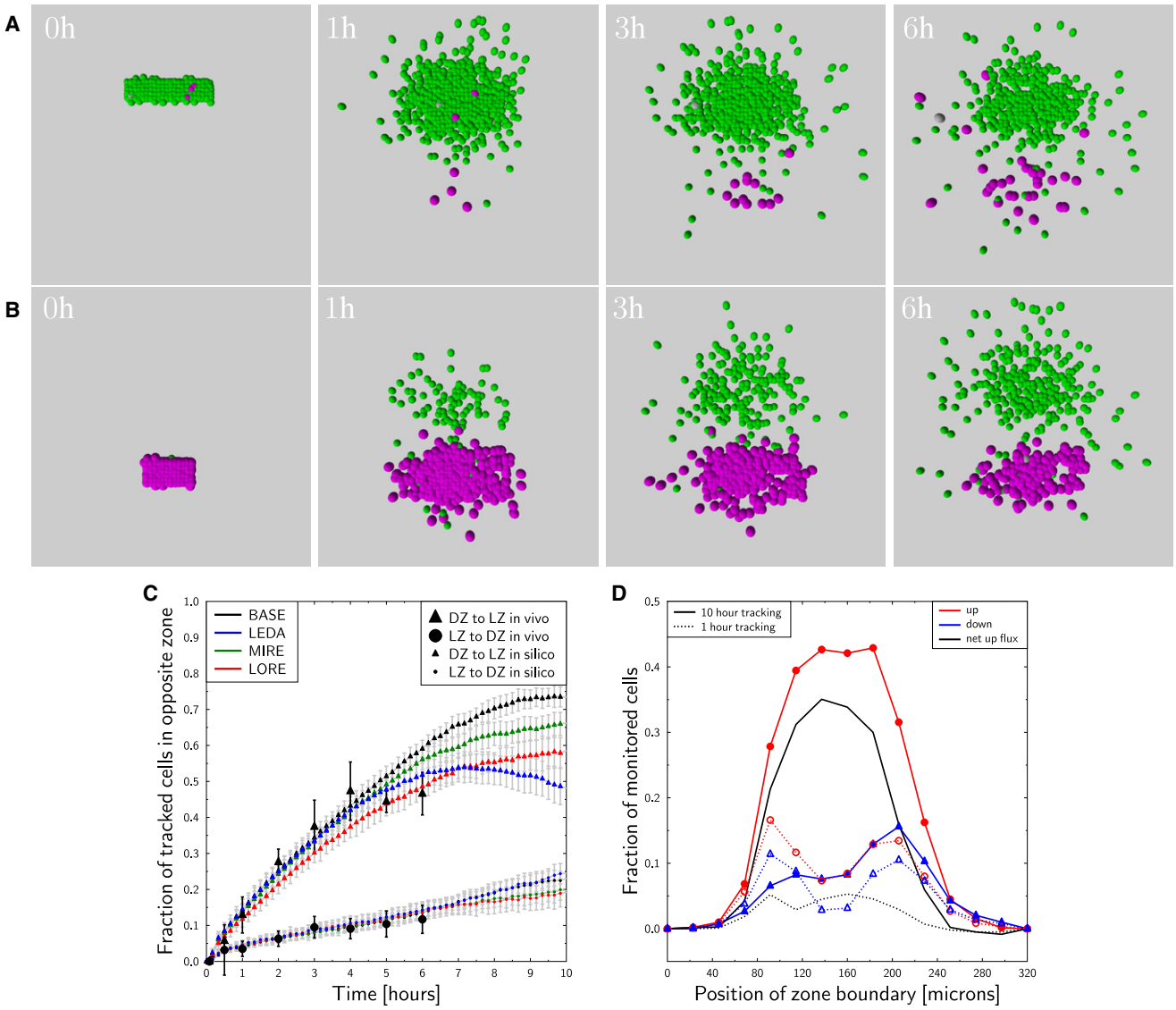

Figure 2. Migration Pattern of Photoactivated BCs

(A–B) BCs were photoactivated in silico at Day 6 after GC onset in volumes of 110 × 110 × 25 μm in the LZ (A) and 60 × 60 × 30 μm in the DZ (B), following the protocol of the in vivo experiment. Both volumes were shifted by 50 μm into the respective zone from the center of the reaction volume. Configurations in the BASE model at the time of photoactivation and 1, 3, and 6 hr later are shown, with the whole GC depth projected onto the image. Color code: DZ BC (magenta), LZ BC (green), and output cells (gray).

(C) Transzone migration events in (A) and (B) were quantified for DZ-to-LZ (triangles) and LZ-to-DZ (circles) transzone migration for the different models (1 SD, N = 30, gray) and compared to the corresponding in vivo data (large symbols).

(D) Transzone migration frequency through a plane at the position given on the horizontal axis in tracking experiments lasting for 10 hr (full lines) and 1 hr (dotted lines) based on 1,000 DZ and 1,000 LZ BCs in the simulation, as shown in (A) and (B). Transmigration from DZ to LZ (red), LZ to DZ (blue), and the net flux from DZ to LZ (black) are shown.

FDCs are located in the central LZ, while BCs searching for TC help concentrate in the outer part of the LZ, where more TFHs are observed (Hardie et al., 1993).

We conclude that the asymmetry of transzone migration frequencies is compatible with the cyclic re-entry model provided that (a) BCs de- and resensitize for chemokines, and (b) upon recycling, BCs enter the cell cycle while still in the LZ.

A Large Recycling Probability Increased Transmigration Asymmetry

The BASE model assumed a recycling probability of 90%; i.e., a positively selected BC differentiates to an output cell with 10% probability, otherwise returning to a DZ proliferative phenotype. Intuitively, a reduced recycling probability would be expected to increase the asymmetry between the two directions of transzone migration. This was tested in the MIRE

(50% recycling) and LORE (20% recycling) models. It is surprising that these models showed that reduced recycling probability led to reduced rather than increased asymmetry.

Less recycling reduced the total number of BCs and the DZ-to-LZ ratio. Compensating for the loss of BCs and restoring DZ to LZ ratio require BC division after each round of selection to be increased, either by increasing the number of divisions per round or by shortening cell cycle duration. Increasing divisions per round of selection was possible only to a limited extent, because this slowed down transmigration from DZ to LZ (as described in the previous section, "Recycled BCs Start the Cell Cycle in the LZ"). Reducing cell cycle duration restored the GC population. Restoration of the DZ to LZ ratio required shorter times BCs spend in the LZ, which in turn increased LZ to DZ transzone migration to rates incompatible with the in vivo data.

We could not identify any solution to this inconsistency. When the recycling probability was set below 50%, high DZ-to-LZ and low LZ-to-DZ transmigration frequency (Figure 2C), a DZ-to-LZ ratio of 2 (Figure 1D), and a stable GC size (Figure 1B) could not be simultaneously generated. This result speaks against the LORE model.

Transmigration Data Suggest that Output Cells Leave the GC through the DZ

Saturation of DZ-to-LZ transzone migration at 50% (Figure 5D in Victora et al., 2010) was not recovered by the BASE model (Figure 2C). As reduced recycling probabilities did not induce sufficient saturation (Figure 2C; green symbols, MIRE), this motivated the development of the LEDA model.

The LEDA model assumed that all BCs selected in the LZ return to the DZ (100% recycling) and divide within this compartment. Following recent experimental results (Thaunat et al., 2012), it is assumed that antigen acquired by BCs is retained by only one of the daughters upon BC division. After two cycles of division in the DZ, those BCs retaining antigen differentiate to output cells and then leave the GC in direction of the T zone, while all other BCs return to the LZ for another round of selection.

One hundred percent recycling increased the LZ-to-DZ transmigration frequency, and the additional division in the DZ increased the DZ-to-LZ ratio (data not shown). Accelerated selection in silico restored the DZ-to-LZ ratio (Figure 1D, in blue) while keeping the LZ-to-DZ transmigration compatible with experiment (Figure 2C, blue dots). DZ-to-LZ transmigration was now limited because a subpopulation of DZ BCs did not migrate back to the LZ but rather exited toward the T zone (Figure 2C, blue triangles). This induced the saturation and even reduction of the fraction of BCs found in the LZ after 8 hr (Figure 2C, blue triangles), because, at that time, BCs that transitioned to the LZ, if selected, were recycled to return to the DZ. This result supports the validity of the LEDA model.

It is interesting that quantitatively correct saturation was only achieved when asymmetric division was restricted to 72% of BC divisions, which is in agreement with the fraction of asymmetric division found in experiment (Figures 2D and S3C in Thaunat et al., 2012). We confirmed that this assumption is consistent with the measured distribution of antigen upon BC divisions in vitro (Figure S1 and Extended Results). The LEDA model results remained stable, when the antigen kept by the BCs staying in the GC was reused in the next round of selection (Figure S2 and Extended Results).

In Situ Plasma Cell Distributions Support the LEDA Model

While the analysis of the photoactivation data (Victora et al., 2010) favors the LEDA model, this novel GC exit theory needs to be strengthened by further experimental data. We therefore investigated whether the spatial distribution of PCs is supportive of an exit path through the DZ.

B10.Br mice were immunized with pigeon cytochrome C (PCC), and the draining lymph nodes were analyzed by confocal microscopy on Day 10 after immunization (Figure 3A). Labeled antibodies for immunoglobulin D (IgD), CD90.2 (Thy1.2) allowed the localization of T zones, BC follicles, and GCs (unstained parts in the follicle). Antibodies against CD138 identified CD138^{high} PCs. These PCs concentrated at the T-B border, i.e., between the DZ and the T zone. The same CD138 pattern was confirmed by immune histology of draining lymph node slices from BALB/c mice at Day 16 after immunization with NP-CGG (Figure 3B).

If the plasmablasts at the T-B border had left the GC through the DZ, it would be expected that a proportion of PC precursors would have upregulated CD138 already in the DZ before actually leaving the GC. However, as plasmablasts upregulate chemokine receptors directing them to the T zone (Pelletier et al., 2010), CD138^{high} cells will not be concentrated in the center of the GC-DZ but will preferentially be localized in the outer part of the DZ. Consequently, GC-central slices are expected to rarely contain CD138^{high} plasmablasts in the center of the DZ, even if a considerable number of CD138^{high} plasmablasts was present in the DZ.

Therefore, CD138^{high} cells in the DZ in some sections and not in the LZ would support the LEDA model. In agreement with this hypothesis, we found CD138^{high} cells in the DZ of GCs of mouse lymph nodes harvested at Day 8 after primary immunization (see Experimental Procedures) with alum precipitated ovalbumin (Figure 3C). Costaining for IgG clearly showed that CD138^{high} PC precursors in the DZ (Figure 3C, red arrows) and in the T-B border are switched (Figure 3C green) and are, thus, likely to be derived from the adjacent GC.

Longer Tracking Times Reveal More Complex Migration Patterns

The accumulation of CD138^{high} PC precursors at the T-B border (Figures 3A–3C) and the existence of CD138^{high} PC precursors in the DZ (Figure 3C) support the notion that plasmablasts leave the GC through the DZ. This encouraged us to search for a clear experimental signature to validate the LEDA model.

One-hour tracking experiments (Allen et al., 2007; Schwickert et al., 2007; Hauser et al., 2007) found small transzone migration frequencies of 5%–10% and a weak asymmetry between both directions of transmigration. In silico (Figure 2D, BASE model), at the zone boundary (160 μm), transzone migration frequencies of 8 and 4% per hour are found for DZ-to-LZ and LZ-to-DZ, respectively. While the asymmetry is small in 1 hr (dotted black line) it is prominent in 10 hr of tracking (full black line) in the very same simulation. This demonstrates that 1 hr tracking experiments are not sensitive for slow GC processes (Meyer-Hermann et al., 2009) such as GC BC death, which lasts about 10 hr according to centrocyte life time (Liu et al., 1989; Liu

Please cite this article in press as: Meyer-Hermann et al., A Theory of Germinal Center B Cell Selection, Division, and Exit, Cell Reports (2012), http://dx.doi.org/10.1016/j.celrep.2012.05.010

Cell PRESS
Open ACCESS

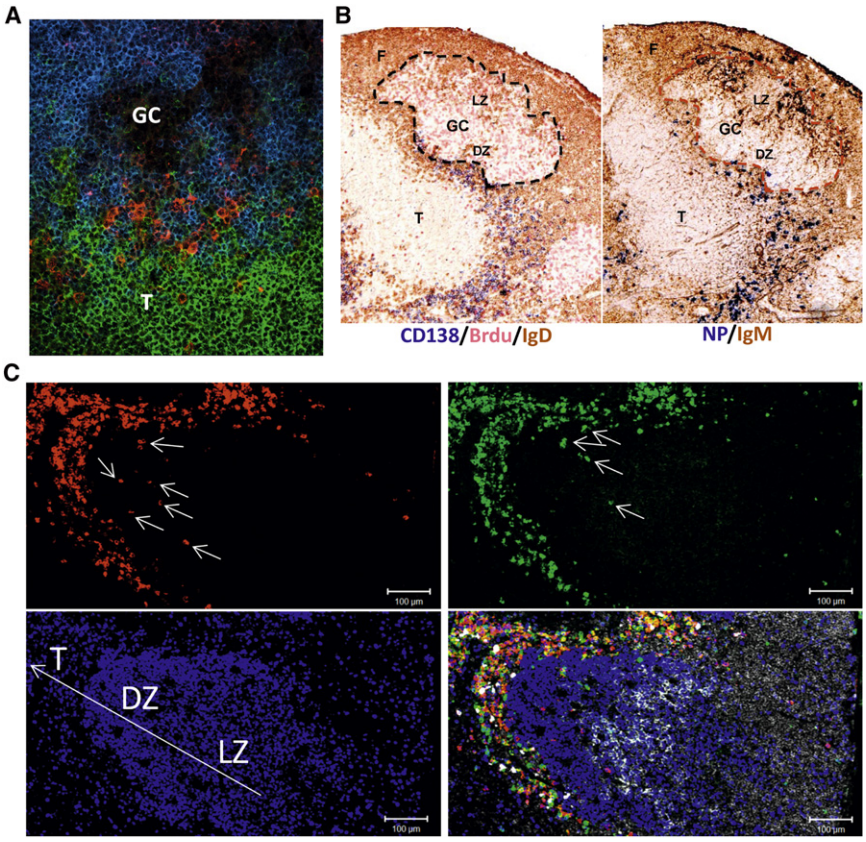

Figure 3. Location of the PCs in Relation to the GC Area

(A) Confocal image of an inguinal lymph node section taken from a wild-type B10.Br mouse 10 days after subcutaneous immunization with PCC protein. The follicular area and the T zone are identified by staining for IgD (blue) and CD90.2 (Thy1.2) (green). GC appear as dark areas within the follicle. CD138^{high} PCs (red) are found predominantly at the T-B border. Magnification, 40×.

(B) Histology of a Day 16 popliteal lymph node taken from a BALB/c mouse after primary immunization in the footpad with NP-CGG in alum plus heat-killed B pertussis. Left: IgD (brown) depicts the follicle where the GCs are located. These contain dividing cells positive for BrdU (pink). CD138^{high} cells (blue) are located at the follicle boundary toward the T zone. Right: Adjacent section showing the same GC stained for NP-specific cells (blue) and IgM (brown). This shows follicular B cells as brown, antigen-specific plasmablasts as dark blue, and the follicular dendritic cell network in the light zone as black.

(C) Confocal images of a Day 8 popliteal lymph node section taken from a mouse that had received transgenic ovalbumin-specific CD4 T cells (OTII) and was immunized in the footpad with alum-precipitated ovalbumin. Ki67 and IgM staining identify the LZ, DZ, and T zone (lower left panel, letters and long arrow from apical GC to T zone): The DZ is characterized by the high density of Ki67^{high}-proliferating BCs (lower left, blue), and absence of IgM (overlay, lower right, white). Staining against IgM (overlay, bottom right, white) highlights the follicular area and immune complexes on FDC in the LZ. CD138^{high} PCs are mainly found at the T-B border (upper left panel, red), and these coincide with IgG1^{high} PCs (upper right, green). Few of these PCs (upper panels, white arrows) are already formed in the GC-DZ. CD138^{high} and IgG1^{high} PCs found in the DZ of the GC are positive for Ki67 and appear in pink (CD138^{high} Ki67^{high}) or cyan (IgG1^{high} Ki67^{high}) on the overlay picture (lower right).

et al., 1994). Note that transmigration through a virtual plane within each zone was larger than at the zone boundary (Figure 2D, dotted red and blue lines). This was in agreement with the findings of Hauser et al., 2007 and resulted in silico from back and forth movement following de- and resensitization to the respective chemokines.

Extending the photoactivation experiment to 2 days showed that the BASE model exhibited dampened oscillation in the transzone migration frequency (Figure 4A), reflecting synchronized movement between zones. Models with lower recycling (MIRE and LORE) equilibrated faster (Figures 4C and 4D). In contrast, in the LEDA model, photoactivated cells accumulated in the DZ (Figure 4B) because all selected BCs returned to the DZ for division, regardless of whether they leave as output cells or recycle back for another round of selection. The qualitative difference between LEDA and other models predicted in silico suggests that they can be distinguished experimentally.

Providing Antigen via DEC205 Receptors

Protein antigens such as ovalbumin (OVA) can be targeted to GC BCs in vivo by fusion to antibodies to the surface lectin DEC205 (Victora et al., 2010). Binding of this fusion protein (anti-DEC205-OVA) to DEC205 receptors on non-OVA-specific BCs allows these cells to internalize OVA and present fragments as pMHC on their surface without BCR crosslinking, enabling the distinction between BCR signaling and T cell help (Victora et al., 2010). Anti-DEC205-OVA treatment of DEC205$^{+/+}$ BCs within a GC composed mainly of DEC205$^{-/-}$ cells (Victora et al., 2010) led to transient accumulation of DEC205$^{+/+}$ cells in the LZ 12 hr post treatment, followed by massive accumulation of these cells in the DZ, concomitant with vigorous proliferation, 1 day later. The GCs re-equilibrate to their initial distribution after 3–4 days (G.D.V., unpublished data). This specific migration pattern is reflected by an oscillation in the DZ-to-LZ ratio (Figure 5B). PC generation is increased by such treatment, but affinity maturation is inhibited.

In order to test the effect of anti-DEC205-OVA injection in silico, the model in Figure 1 was extended to distinguish between DEC205$^{+/+}$ and DEC205$^{-/-}$ BCs. DEC205$^{+/+}$ BCs were loaded with antigen by anti-DEC205-OVA treatment in silico. The selective advantage given to DEC205$^{+/+}$ BCs was modeled as (1) no need to collect antigen from FDCs and (2) the highest probability of TFH signaling. We assumed that loaded DEC205$^{+/+}$ BCs had a 2- to 3-fold higher probability of receiving productive TFH signaling.

Following the experimental setup (Victora et al., 2010), 20% of BCs were assumed to be DEC205$^{+/+}$. Anti-DEC205-OVA was injected at Day 5 after GC onset, and affected all not yet

Cell PRESS
Open ACCESS

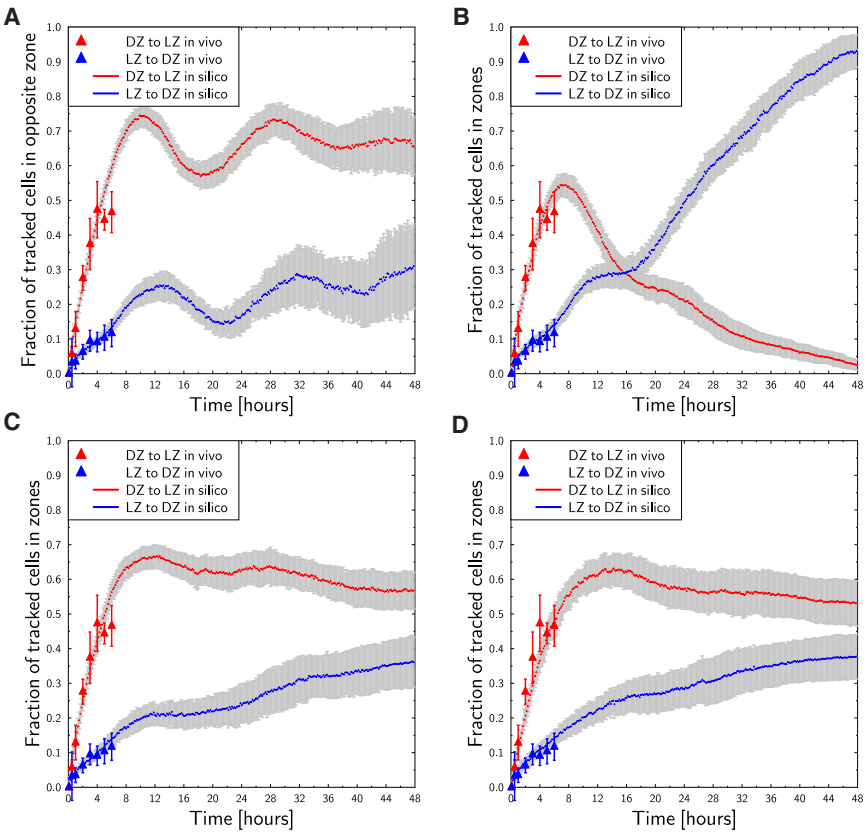

Figure 4. Long-Term Photoactivation Experiment In Silico

Cells were photoactivated at day 6 and tracked for 48 hr using model BASE (A), LEDA (B), MIRE (C), and LORE (D). The symbols show the 6 hr in vivo experiment (Victora et al., 2010).

positively selected LZ BCs. The duration of its effect was set to 24 hr, such that all DZ BCs adopting the LZ phenotype within this time interval also acquired the selective advantage.

BCs Interact Longer with TCs and Sensitize Later for CXCL12

As in silico injection of anti-DEC205-OVA alone induced only a weakly increased DZ-to-LZ ratio but not its initial reduction (data not shown), we investigated potential mechanisms by which we could induce accumulation of BCs in the LZ as seen in vivo.

In agreement with experimental control data (Victora et al., 2010), forced differentiation of DZ BCs to the LZ phenotype in response to anti-DEC205-OVA injection did not induce BC accumulation in the LZ (data not shown) and was thus ruled out. Delayed sensitization to CXCL12 upon DEC205 treatment induced accumulation of BCs in the LZ but not to a sufficient extent (data not shown). However, if in addition to delayed sensitization, we prolonged the phase of TC-BC interaction to 5 hr, the drop in the DZ-to-LZ ratio could be reproduced in all models (Figures 5A and 5B). In silico, prolonged single BC-TC interactions could not be distinguished from a prolonged phase of BC collection of signals integrated from short contacts to different TCs.

High-Affinity TC Signals Increase BC Division and Reduce Recycling

Thirty-six hours after anti-DEC205-OVA injection in vivo, the LZ was depleted of DEC205$^{+/+}$ BCs, which instead accumulated in the DZ, leading to a 10-fold increase in the DZ-to-LZ ratio. While all in silico models exhibited an increased DZ-to-LZ ratio after injection, none was in quantitative agreement (data not shown). Such extreme ratios were only achieved if the abundant TC help triggered by anti-DEC205-OVA targeting induced five to six divisions in positively selected DEC205$^{+/+}$ BCs (Figures 5A and 5B).

Prolonging the phase of TC-BC interactions increased competition for TC help (Figure 6A) and, therefore, also the selective pressure on DEC205$^{-/-}$ BCs. This strongly increased the fraction of DEC205$^{+/+}$ BCs to above 90%, in contradiction to the values of around 70% found at 48 hr in vivo (Figure 6D in Victora et al., 2010). Restoring this readout required reducing the recycling probability for selected DEC205$^{+/+}$ BCs (Figure 5C). BASE required a reduction from 90% to 45%, MIRE from 50% to 10%, and LEDA from 100% to 30%, where the 70% BCs primed to differentiate into output divide in the DZ before leaving the GC. In contrast, the LORE model had less flexibility in recycling (Figure 6B, in red) and was in contradiction to the data: The fraction of DEC205$^{+/+}$ BCs could only be restored by reducing the number of divisions but at the price of an excessively low DZ-to-LZ ratio at 48 hr posttreatment (Figure 5B, in red) and a strongly reduced GC population (data not shown).

When starting from 30% DEC205$^{+/+}$ BCs, the fraction of DEC205$^{+/+}$ BCs increased to 90% upon anti-DEC205-OVA injection in vivo (Victora et al., 2010, Figure 7B). Assuming the same reduced recycling probability as mentioned earlier, this value is reproduced in silico in all but the LORE model (data not shown).

In conclusion, the in silico models predicted that BCs with artificially increased antigen presentation enter a prolonged phase of interaction with TCs, during which BCs are positively selected, receive a strong proliferation signal from TCs, downregulate recycling (correspondingly upregulate differentiation to output cells), and exhibit retarded sensitization to CXCL12.

Impact of Anti-DEC205-OVA on Affinity Maturation and Output Cell Generation

Having at hand a simulation adequately reflecting the experimental findings of Victora et al. (2010), we proceeded to probe the impact of anti-DEC205-OVA injection on affinity maturation.

Please cite this article in press as: Meyer-Hermann et al., A Theory of Germinal Center B Cell Selection, Division, and Exit, Cell Reports (2012), http://dx.doi.org/10.1016/j.celrep.2012.05.010

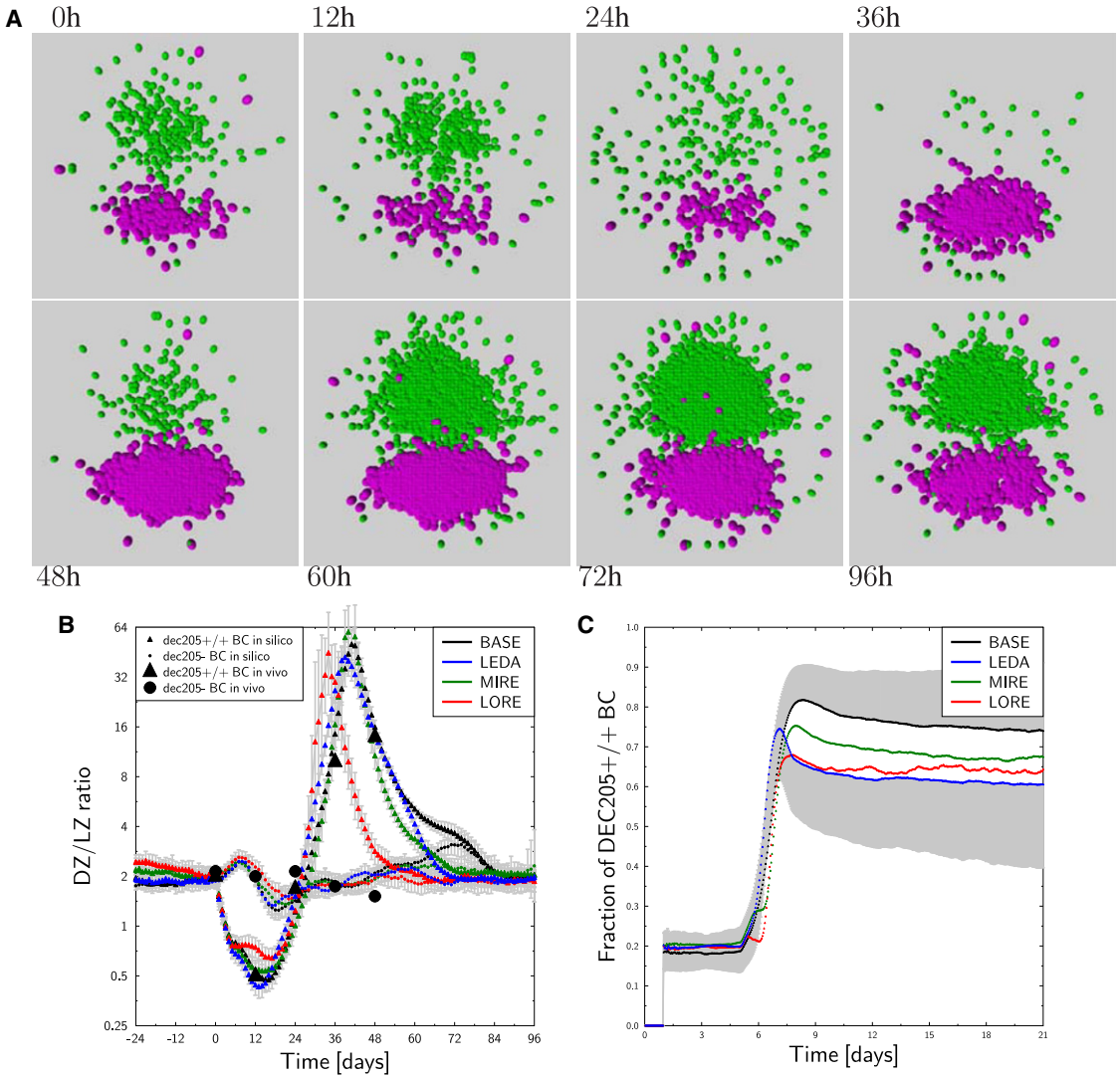

Figure 5. Anti-DEC205-OVA Treatment In Silico

(A) Projection of all DEC205$^{+/+}$ BCs before treatment (0 hr) and in the following 4 days are shown for the BASE model. The GC was initiated with 20% DEC205$^{+/+}$ BCs, and anti-DEC205-OVA was injected at Day 5 and remained available for 24 hr. DEC205-OVA-competent TC-BC interactions were prolonged to 5 hr, triggered 5.4 divisions, reduced the recycling probability to 45%, and delayed sensitization for CXCL12 by 10 hr. Color code: dividing BC (magenta), nondividing BC (green).

(B) DZ-to-LZ ratio in response to anti-DEC205-OVA injection (at time 0) in vivo (large symbols; Victora et al., 2010, Figure 6C) for DEC205$^{+/+}$ (triangles) and DEC205$^{-/-}$ (circles) BCs and in silico (small symbols) in the models BASE (black), LEDA (blue), MIRE (green), and LORE (red).

(C) Fraction of DEC205$^{+/+}$ BCs compared to 70% found in vivo 48 hr postinjection (Victora et al., 2010, Figure 6D). Half error bars are shown for BASE and LEDA only. Color code is as in (B).

A Second Phase of Monoclonal Expansion. The fraction of recycling events in LZ BCs was reduced during the phase of accumulation of BCs in the LZ (Figure 6B). DEC205$^{+/+}$ BCs were retained in the LZ in a prolonged phase of competition for TC help (Figure 6A). The inhibition of recycling events was counter-acted by the subsequent push in recycling when the DZ was repopulated by dividing BCs. The fraction of recycling events subsequently dropped again because the increased number of divisions in the DZ delayed re-entry to the LZ (Figure 6B). In this phase, the number of GC BCs increased without any affinity-based selection, in a process reminiscent of the initial phase of monoclonal expansion.

Affinity Maturation Is Well Described without Anti-DEC205-OVA Injection. The fraction of high-affinity antibody-producing output cells (Figure 6C) was monitored as a measure of the fraction of high-affinity antibodies in serum (NP3/NP23 ratio in Victora et al., 2010, Figure 7G). In agreement with the experimental results, affinity maturation continuously increased in silico, reaching saturation after 3 weeks in all models (Figure 6C, thin lines).

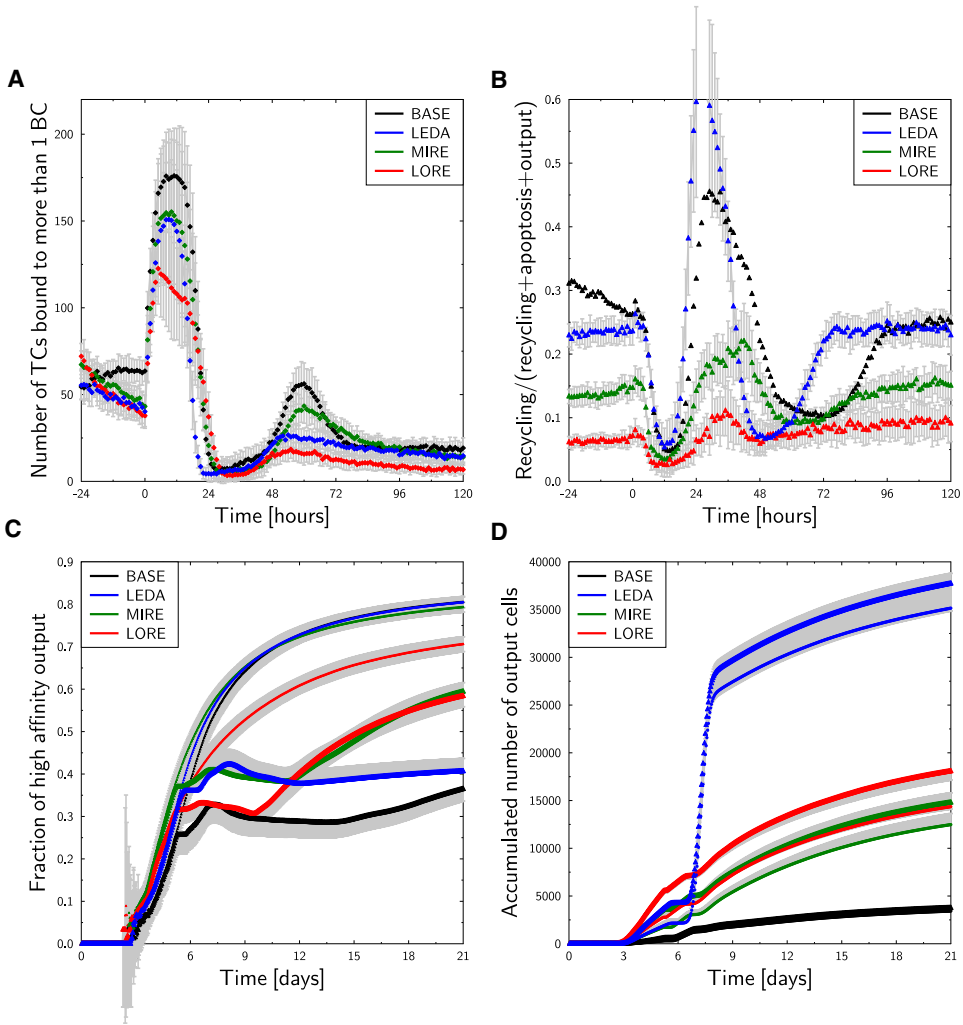

Figure 6. Selection and Affinity Maturation upon Anti-DEC205-OVA Injection

GC characteristics were analyzed starting from 20% (A and B), 100% (C), and 50% (D) DEC205$^{+/+}$ BCs in response to a single anti-DEC205-OVA injection using the different in silico models BASE (black), LEDA (blue), MIRE (green), and LORE (red).

(A) Number of TCs in contact to more than one BC.

(B) Fraction of recycling events among LZ BCs.

(C) Fraction of high-affinity output cells in an experiment starting from 100% DEC205$^{+/+}$ BCs without (thin lines) and with thick lines repeated anti-DEC205-OVA injection.

(D) Total number of GC-derived output cells (thick lines) and total number of DEC205$^{+/+}$ output cells (thin lines).

Anti-DEC205-OVA Injection Inhibits Affinity Maturation Also In Silico. Upon repeated injection of anti-DEC205-OVA in vivo into wild-type GCs containing 100% endogenous DEC205$^{+/+}$ BCs, affinity maturation was suppressed and did not recover (Victora et al., 2010, Figure 7G). This was also found in silico (Figure 6C). However, with LORE and MIRE, affinity recovered when the effect of anti-DEC205-OVA ceased after 4 days. A long-term inhibition of affinity maturation was recapitulated in BASE and LEDA only (Figure 6C, thick black and blue lines).

Anti-DEC205-OVA Injection Increased Output Cell Generation. In vivo, upon anti-DEC205-OVA injection, the total number of PCs increased by more than 10-fold compared to control experiments (Victora et al., 2010, Figure 7F, using 50% DEC205$^{+/+}$ BCs). In silico, the number of output cells was increased in all models (Figure 6D) but only in the LEDA model to a sufficient extent (Figure 6D, thick blue line, steep vertical increase). As observed in vivo, the largest part of this increase in output cell number was related to the DEC205$^{+/+}$ BC compartment (Figure 6D, thin blue line).

DISCUSSION

The present analysis combined a large body of experimental data into a state-of-the-art in silico model of the GC reaction, the LEDA model. This theory enabled us to define the most relevant mechanisms at action in GC reactions and to predict the outcome of future experiments aimed at testing this novel exit hypothesis. According to the LEDA model, BCs acquire,

process, and present antigen from FDCs and compete for TFH help. Interaction with TFHs and subsequent intracellular BC signaling determine the fate of the BCs in the LZ: LEDA predicts that the higher the pMHC density on the BCs, the more BC divisions are induced and the more the mutation frequency is reduced. Noncompetitive BCs die by apoptosis. LEDA further predicts that selected BCs enter the S phase in the LZ but return to the DZ before reaching the G2/M phase of the cell cycle. Recent data suggested that asymmetric distribution of the antigen onto the daughter cells is fate decisive (Thaunat et al., 2012). LEDA predicts that the antigen-retaining subset of BCs enters final differentiation. Most important, this involves the prediction of a new GC exit model, according to which selected BCs divide in the DZ before leaving the GC in direction of the adjacent T zone. BCs without antigen return to the LZ for a further round of antigen acquisition and selection. This summary of the new model guides through the following discussion.

Reproducing in silico the experimental results in which antigen is provided to GC BCs by DEC205 targeting required (1) a prolonged phase of DEC205$^{+/+}$ BC interactions with TFH, (2) delayed sensitization to CXCL12, (3) five to six rounds of division among BCs positively selected by TFHs, and (4) a reduction of the recycling probability of positively selected BCs. This result suggests that TFHs control both, recycling and division, in an affinity-dependent manner (Iber and Maini, 2002; Meyer-Hermann, 2007; Turner et al., 2008) and that these parameters may change dynamically during the course of the GC reaction.

It is interesting that these effects coincide with BC characteristics found during the initiation process of T-dependent GCs. Longer TC-BC interactions were observed during the initiation phase at the border of the T zone and the BC follicle (Allen et al., 2007). These interactions gave rise to a pronounced generation of early PCs (Schwickert et al., 2011). Activated BCs that did not enter the PC pool remained CXCL13 sensitive for a longer period in order to re-enter the follicle. There they underwent a phase of monoclonal expansion including about six cell divisions and generated the base population of the GC reaction (Liu et al., 1991). This suggests that the intense BC-TC interaction induced by anti-DEC205-OVA in a later phase of an ongoing GC reaction might reset BCs to a state similar to that of GC seeder cells. This is further supported by the observation that the early TC-BC interactions at the T-B border were also dependent on pMHC density (Schwickert et al., 2011). However, differences in Fas expression between anti-DEC205-OVA treated and GC seeder cells (Victora et al., 2010) still reflect that the former BCs were not activated for the first time but were already part of an ongoing GC.

A control of the mutation rate (Dustin and Meyer-Hermann, 2012) via activation of the Akt kinase (Chaturvedi et al., 2011) and subsequent inhibition of activation induced cytosine deaminase (Omori et al., 2006) is an attractive speculation. While not being required in silico for consistency with experiment, the simulations predict that a control of the frequency of somatic hypermutation by antibody affinity would optimize affinity maturation.

The in silico analysis of the in vivo transzone migration data implies that BCs enter the cell cycle in the LZ immediately after selection, such that, by the time these cells enter the DZ, they have already completed a part of the S phase of the cell cycle. In accordance with this prediction, Ki67-positive, BrdU-labeled, and S-phase BCs have been detected in the LZ (Liu et al., 1992; Camacho et al., 1998; Meyer-Hermann and Maini, 2005; Allen et al., 2007; Hauser et al., 2007; Meyer-Hermann et al., 2009; Victora et al., 2010), while mitotic BCs were found mostly in the DZ (Victora et al., 2010).

The present analysis of the measured tranzone migration frequencies revealed that positively selected BCs dominantly recycle to reproliferating BCs. Models with recycling probabilities below 50% failed to recapitulate the experimental data such that transzone migration, DZ-to-LZ ratio, and GC population dynamics could not be simultaneously reproduced. In addition, the progression of the DZ-to-LZ ratio in response to injection of anti-DEC205-OVA was poorly reflected (Figure 5B).

Asymmetric distribution of retained antigen in dividing GC BCs (in 72% of the cases) is an appealing mechanism to determine which BCs are selected for final differentiation (LEDA model). This mechanism can be replaced by the LEDAX model in which, after symmetric divisions in the DZ, a probabilistic decision is made as to whether a BC differentiates to output or heads for another round of selection. This decision might reflect previous interaction signals received from TFH in the LZ. The difference between both model readouts is not significant, such that both are supported by the present analysis. On one hand, in vitro data suggest that the fate of BCs may not be triggered by cell-cell contact or asymmetric division but would be a result of stochastic decisions whereby the probabilities for the BC fate are derived from unspecific signals in the GC environment (Duffy et al., 2012). If this remained valid for antigen-loaded BCs, such an idea would support the LEDAX model. On the other hand, the recent finding that BCs, indeed, divide asymmetrically three out of four times (Thaunat et al., 2012) favors the LEDA model. The recent observation that the transcription factor Bcl-6 and the interleukin-21 receptor are also asymmetrically distributed in dividing BCs (Barnett et al., 2012) suggests an even more differentiated regulation of BC fates by asymmetric distribution of key molecules. Note that both models predict a mechanism for GC PC generation. Memory BCs are generated with dynamics that differ from long-lived PCs (Smith et al., 1997; Purtha et al., 2011) and need to be investigated separately.

How strong is the evidence for the LEDA model? Motility, morphology, phenotype, and transzone migration data were reproduced by both the BASE and the LEDA models. LEDA was further supported by its capturing of the saturation of transzone migration data (Figure 2B) and by the substantial increase in the number of output cells in response to anti-DEC205-OVA injection (Figure 6D; Figure 7F in Victora et al., 2010). LEDA predicts that PC precursors divide in the DZ before actually upregulating CD138 and leaving the GC. Consistent with this prediction, Ki67-positive plasmablasts were found to gradually decrease in numbers with distance from the GC DZ in the direction of the lymph node medulla (Mohr et al., 2009). Markers related to PC differentiation were correspondingly upregulated (Mohr et al., 2009). In this model, IRF-4 and Blimp-1 positive cells found in the LZ (Cattoretti et al., 2006) would be considered as PC precursor cells that subsequently migrate to the DZ and then

further to the T zone in response to CXCL12. LEDA is further supported by the detection of $CD138^{high}$ cells in the GC-DZ, especially near the T-B border (Figure 3). This is the expected pattern if PC precursors leave the GC through the DZ. It was previously shown that PCs accumulating at the T-B border interact with TCs and may control recruitment of TFHs to GCs (Pelletier et al., 2010). This finding could provide a clue for the relevance of plasmablast exit through the DZ.

Further investigation is required to definitely identify the origin and path of post-GC PCs in the lymph node. The ultimate aim, i.e., the direct observation of positively selected BCs starting in the LZ, following through migration to the DZ, division within this compartment, and exit from the GC in direction of the T zone, is impossible with current technology. The present analysis showed that, alternatively, the LEDA model could be validated by tracking transzonal migration for a period of 2 days. After photoactivation of BCs in any zone, the majority of highlighted cells are predicted to be concentrated in the DZ in the LEDA(X) model but not in the other three models, which predict equilibration between the two zones at 50% (Figure 4). The reason for this is that, in the classical cyclic re-entry models, BCs undergo multiple rounds of mutation and selection and, thus, oscillate between zones. In the LEDA model, cells programmed to become output cells accumulate in the DZ after every round of selection. This prediction of a conclusive experiment is in the spirit of the iterative communication between theory and experiment in physics. However, novel experimental techniques are required to allow for long-term tracking of in-situ-labeled cells.

The predicted LEDA theory of GCs has major implications for the number and timing of PC generation and, by this, has consequences to human health. The number of PCs generated by vaccination, is often not satisfying, especially in the elderly. In LEDA, the number of PCs generated is improved by an order of magnitude, because every selection event generates one PC, whereas in other models, depending on the recycling probability, only every second to 10^{th} selection event generates a PC. In LEDA, affinity maturation appears also faster than in other models (Figure 1F; one day compared to BASE), because, in contrast to other GC models, the information about improved clones is kept in the GC by means of asymmetric division. Unlike in other models, PCs exiting the GC leave a copy of themselves in the GC and, by this, optimize information processing in the GC reaction. Both timing and number of PCs are a direct consequence of asymmetric division, which might be a suitable target to control or optimize GC efficiency.

EXPERIMENTAL PROCEDURES

The present in silico simulations were made with a newly developed stochastic event generator in which each cell is individually represented and can adopt different states of differentiation, mutation, division, and position. A large diversity of experimental constraints (morphology, population kinetics, duration of processes, cell motility, cell-cell-interaction) were used to determine the model's properties. The basic philosophy of the model is to implement known mechanisms and to use the mathematical model for the analysis of the whole interacting system. Thus, the read-outs of the system are not set by hand but instead emerge from the implemented mechanisms described in the Extended Experimental Procedures.

For Figure 3A, wild-type B10.Br mice were immunized subcutaneously with 400 μg of PCC protein (Sigma) in Ribi adjuvant (lab formulation based on Baldridge and Crane, 1999). Inguinal lymph nodes from three different mice were harvested 10 days after primary immunization, embedded in OCT compound (Sakura), and snap-frozen on dry ice. Tissue section of 6 to 8 μm were air dried, fixed in cold acetone, and stored at −20°C until staining. Stainings were performed in PBS, 10% fetal calf serum, 0.1% azide with anti-IgD APC (11.26, labeled in the laboratory), anti-CD90.2 fluorescein isothiocyanate (FITC) (53-2.1, BD Biosciences), and purified anti-CD138 (281.2, BD Biosciences). CD138 staining was revealed with biotinylated antirat immunoglobulin G (IgG) (vector) and rhodamin red streptavidin (Invitrogen). Confocal images were analyzed with an Olympus Fluoview 500 confocal microscope.

For Figure 3B, BALB/c mice were immunized in the footpad with NP-CGG in alum plus heat-killed B pertussis. The mice received 5-bromo-2′deoxyuridine (BrdU) 2 hr before sacrifice at Day 16. The popliteal lymph node was prepared as described in Toellner et al. (1998) and stained for IgD, BrdU, and CD138.

For Figure 3C, the staining was done on at least three lymph nodes each harvested in independent experiments. For adoptive transfer, 5×10^6 cells from the lymph nodes of OT-II mice, transgenic for αβ TC-receptor specific for OVA323-339 peptide in the context of H-2 I-Ab (Charles River Breeding Laboratories), were injected intravenously into congenic wild-type 5- to 7-week-old C57BL/6J recipients. Mice were immunized with alum-precipitated ovalbumin subcutaneously into the rear footpad, as previously described (Mohr et al., 2009). Day 8 after immunization, snap-frozen popliteal lymph nodes were prepared, and 6 μm sections were cut, fixed, and stained as previously described (Mohr et al., 2009). Confocal images were acquired using a Zeiss LSM510 laser scanning confocal microscope with a Zeiss AxioVert 100M microscope equipped with 10× objective. The following reagents were used: FITC-conjugated goat antimouse IgG1 (Southern Biotech), rat antimouse CD138 biotin (BD PharMingen) plus Cy3-conjugate streptavidin, rabbit anti-Ki67 (a kind gift from Johannes Guerdes, Borstel) plus Cy5-conjugated donkey antirabbit IgG (Jackson Immunoresearch), and aminomethylcoumarin acetate-conjugated (AMCA) goat antimouse immunoglobulin M (IgM). Signals obtained from these four markers were scanned separately and stored in four nonoverlapping channels as pixel digital arrays of 2,048 × 2,048.

All animal experiments were approved according to local ethical committee and home office guidelines.

SUPPLEMENTAL INFORMATION

Supplemental Information includes Extended Results, Extended Experimental Procedures, two figures, and one table and can be found with this article online at http://dx.doi.org/10.1016/j.celrep.2012.05.010.

LICENSING INFORMATION

ACKNOWLEDGMENTS

We thank Mike Dustin, Michel Nussenzweig, and Michael McHeyzer-Williams for intense discussions and valuable comments on science and the manuscript. M.M.-H. was supported by the BMBF (GerontoMitoSys and GerontoShield in the GerontoSys Initiative) and by the HFSP. E.M. was supported by FCT (Fundação para a Ciência e Tecnologia).

Received: January 25, 2012
Revised: March 22, 2012
Accepted: May 15, 2012
Published online: June 28, 2012

REFERENCES

Allen, C.D., Okada, T., Tang, H.L., and Cyster, J.G. (2007). Imaging of germinal center selection events during affinity maturation. Science *315*, 528–531.

Baldridge, J.R., and Crane, R.T. (1999). Monophosphoryl lipid A (MPL) formulations for the next generation of vaccines. Methods *19*, 103–107.

Barnett, B.E., Ciocca, M.L., Goenka, R., Barnett, L.G., Wu, J., Laufer, T.M., Burkhardt, J.K., Cancro, M.P., and Reiner, S.L. (2012). Asymmetric B cell division in the germinal center reaction. Science *335*, 342–344.

Beltman, J.B., Allen, C.D.C., Cyster, J.G., and de Boer, R.J. (2011). B cells within germinal centers migrate preferentially from dark to light zone. Proc. Natl. Acad. Sci. USA *108*, 8755–8760.

Berek, C., and Milstein, C. (1987). Mutation drift and repertoire shift in the maturation of the immune response. Immunol. Rev. *96*, 23–41.

Berek, C., Berger, A., and Apel, M. (1991). Maturation of the immune response in germinal centers. Cell *67*, 1121–1129.

Camacho, S.A., Kosco-Vilbois, M.H., and Berek, C. (1998). The dynamic structure of the germinal center. Immunol. Today *19*, 511–514.

Cattoretti, G., Shaknovich, R., Smith, P.M., Jäck, H.-M., Murty, V.V., and Alobeid, B. (2006). Stages of germinal center transit are defined by B cell transcription factor coexpression and relative abundance. J. Immunol. *177*, 6930–6939.

Chaturvedi, A., Martz, R., Dorward, D., Waisberg, M., and Pierce, S.K. (2011). Endocytosed BCRs sequentially regulate MAPK and Akt signaling pathways from intracellular compartments. Nat. Immunol. *12*, 1119–1126.

Depoil, D., Zaru, R., Guiraud, M., Chauveau, A., Harriague, J., Bismuth, G., Utzny, C., Müller, S., and Valitutti, S. (2005). Immunological synapses are versatile structures enabling selective T cell polarization. Immunity *22*, 185–194.

Duffy, K.R., Wellard, C.J., Markham, J.F., Zhou, J.H., Holmberg, R., Hawkins, E.D., Hasbold, J., Dowling, M.R., and Hodgkin, P.D. (2012). Activation-induced B cell fates are selected by intracellular stochastic competition. Science *335*, 338–341.

Dunn-Walters, D.K., Belelovsky, A., Edelman, H., Banerjee, M., and Mehr, R. (2002). The dynamics of germinal centre selection as measured by graph-theoretical analysis of mutational lineage trees. Dev. Immunol. *9*, 233–243.

Dustin, M.L., and Meyer-Hermann, M. (2012). Immunology. Antigen feast or famine. Science *335*, 408–409.

Figge, M.T., Garin, A., Gunzer, M., Kosco-Vilbois, M., Toellner, K.-M., and Meyer-Hermann, M. (2008). Deriving a germinal center lymphocytemigration-model from two-photon data. J. Exp. Med. *205*, 319–329.

Fleire, S.J., Goldman, J.P., Carrasco, Y.R., Weber, M., Bray, D., and Batista, F.D. (2006). B cell ligand discrimination through a spreading and contraction response. Science *312*, 738–741.

Hanna, M.G., Jr. (1964). An autoradiographic study of the germinal center in spleen white pulp during early intervals of the immune response. Lab. Invest. *13*, 95–104.

Hardie, D.L., Johnson, G.D., Khan, M., and MacLennan, I.C. (1993). Quantitative analysis of molecules which distinguish functional compartments within germinal centers. Eur. J. Immunol. *23*, 997–1004.

Hauser, A.E., Junt, T., Mempel, T.R., Sneddon, M.W., Kleinstein, S.H., Henrickson, S.E., von Andrian, U.H., Shlomchik, M.J., and Haberman, A.M. (2007). Definition of germinal-center B cell migration in vivo reveals predominant intrazonal circulation patterns. Immunity *26*, 655–667.

Hollowood, K., and Macartney, J. (1992). Cell kinetics of the germinal center reaction—a stathmokinetic study. Eur. J. Immunol. *22*, 261–266.

Iber, D., and Maini, P.K. (2002). A mathematical model for germinal centre kinetics and affinity maturation. J. Theor. Biol. *219*, 153–175.

Jacob, J., Kelsoe, G., Rajewsky, K., and Weiss, U. (1991). Intraclonal generation of antibody mutants in germinal centres. Nature *354*, 389–392.

Kepler, T.B., and Perelson, A.S. (1993). Cyclic re-entry of germinal center B cells and the efficiency of affinity maturation. Immunol. Today *14*, 412–415.

Keşmir, C., and De Boer, R.J. (1999). A mathematical model on germinal center kinetics and termination. J. Immunol. *163*, 2463–2469.

Kosco-Vilbois, M.H. (2003). Are follicular dendritic cells really good for nothing? Nat. Rev. Immunol. *3*, 764–769.

Liu, Y.J., Joshua, D.E., Williams, G.T., Smith, C.A., Gordon, J., and MacLennan, I.C. (1989). Mechanism of antigen-driven selection in germinal centres. Nature *342*, 929–931.

Liu, Y.J., Zhang, J., Lane, P.J., Chan, E.Y., and MacLennan, I.C.M. (1991). Sites of specific B cell activation in primary and secondary responses to T cell-dependent and T cell-independent antigens. Eur. J. Immunol. *21*, 2951–2962.

Liu, Y.J., Johnson, G.D., Gordon, J., and MacLennan, I.C.M. (1992). Germinal centres in T-cell-dependent antibody responses. Immunol. Today *13*, 17–21.

Liu, Y.J., Barthelemy, C., de Bouteiller, O., and Banchereau, J. (1994). The differences in survival and phenotype between centroblasts and centrocytes. Adv. Exp. Med. Biol. *355*, 213–218.

MacLennan, I.C.M. (1994). Germinal centers. Annu. Rev. Immunol. *12*, 117–139.

Meyer-Hermann, M. (2007). A concerted action of B cell selection mechanisms. Adv. Complex Syst. *10*, 557–580.

Meyer-Hermann, M., Figge, M.T., and Toellner, K.M. (2009). Germinal centres seen through the mathematical eye: B-cell models on the catwalk. Trends Immunol. *30*, 157–164.

Meyer-Hermann, M.E., and Maini, P.K. (2005). Cutting edge: back to "one-way" germinal centers. J. Immunol. *174*, 2489–2493.

Meyer-Hermann, M.E., Maini, P.K., and Iber, D. (2006). An analysis of B cell selection mechanisms in germinal centers. Math. Med. Biol. *23*, 255–277.

Mohr, E., Serre, K., Manz, R.A., Cunningham, A.F., Khan, M., Hardie, D.L., Bird, R., and MacLennan, I.C.M. (2009). Dendritic cells and monocyte/macrophages that create the IL-6/APRIL-rich lymph node microenvironments where plasmablasts mature. J. Immunol. *182*, 2113–2123.

Omori, S.A., Cato, M.H., Anzelon-Mills, A., Puri, K.D., Shapiro-Shelef, M., Calame, K., and Rickert, R.C. (2006). Regulation of class-switch recombination and plasma cell differentiation by phosphatidylinositol 3-kinase signaling. Immunity *25*, 545–557.

Pelletier, N., McHeyzer-Williams, L.J., Wong, K.A., Urich, E., Fazilleau, N., and McHeyzer-Williams, M.G. (2010). Plasma cells negatively regulate the follicular helper T cell program. Nat. Immunol. *11*, 1110–1118.

Purtha, W.E., Tedder, T.F., Johnson, S., Bhattacharya, D., and Diamond, M.S. (2011). Memory B cells, but not long-lived plasma cells, possess antigen specificities for viral escape mutants. J. Exp. Med. *208*, 2599–2606.

Radmacher, M.D., Kelsoe, G., and Kepler, T.B. (1998). Predicted and inferred waiting times for key mutations in the germinal centre reaction: evidence for stochasticity in selection. Immunol. Cell Biol. *76*, 373–381.

Schwickert, T.A., Lindquist, R.L., Shakhar, G., Livshits, G., Skokos, D., Kosco-Vilbois, M.H., Dustin, M.L., and Nussenzweig, M.C. (2007). In vivo imaging of germinal centres reveals a dynamic open structure. Nature *446*, 83–87.

Schwickert, T.A., Victora, G.D., Fooksman, D.R., Kamphorst, A.O., Mugnier, M.R., Gitlin, A.D., Dustin, M.L., and Nussenzweig, M.C. (2011). A dynamic T cell-limited checkpoint regulates affinity-dependent B cell entry into the germinal center. J. Exp. Med. *208*, 1243–1252.

Smith, K.G., Light, A., Nossal, G.J., and Tarlinton, D.M. (1997). The extent of affinity maturation differs between the memory and antibody-forming cell compartments in the primary immune response. EMBO J. *16*, 2996–3006.

Tarlinton, D.M., and Smith, K.G. (2000). Dissecting affinity maturation: a model explaining selection of antibody-forming cells and memory B cells in the germinal centre. Immunol. Today *21*, 436–441.

Thaunat, O., Granja, A.G., Barral, P., Filby, A., Montaner, B., Collinson, L., Martinez-Martin, N., Harwood, N.E., Bruckbauer, A., and Batista, F.D. (2012). Asymmetric segregation of polarized antigen on B cell division shapes presentation capacity. Science *335*, 475–479.

Toellner, K.-M., Luther, S.A., Sze, D.M.-Y., Choy, R.K.-W., Taylor, D.R., MacLennan, I.C.M., and Acha-Orbea, H. (1998). T helper 1 (Th1) and Th2 characteristics start to develop during T cell priming and are associated with an immediate ability to induce immunoglobulin class switching. J. Exp. Med. *187*, 1193–1204.

Turner, M.L., Hawkins, E.D., and Hodgkin, P.D. (2008). Quantitative regulation of B cell division destiny by signal strength. J. Immunol. *181*, 374–382.

Victora, G.D., and Nussenzweig, M.C. (2012). Germinal centers. Annu. Rev. Immunol. *30*, 429–457.

Victora, G.D., Schwickert, T.A., Fooksman, D.R., Kamphorst, A.O., Meyer-Hermann, M., Dustin, M.L., and Nussenzweig, M.C. (2010). Germinal center dynamics revealed by multiphoton microscopy with a photoactivatable fluorescent reporter. Cell *143*, 592–605.

Zhang, J., MacLennan, I.C.M., Liu, Y.J., and Lane, P.J. (1988). Is rapid proliferation in B centroblasts linked to somatic mutation in memory B cell clones? Immunol. Lett. *18*, 297–299.